AGU PUBLICATIONS

Geophysical Research Letters

RESEARCH LETTER
10.1002/2016GL068250

Key Points:
- A 1 month transient event (*Mw* 5.3) has been detected by high temporal resolution InSAR time series along the North Anatolian Fault
- A Bayesian inversion constrains the depth (between 0 and 3 km), the length (8 km), and the peak slip (2 cm) of this transient event
- A need for a revision of the current mechanical model of this segment is highlighted

Supporting Information:
- Supporting Information S1

Correspondence to:
B. Rousset,
baptiste.rousset@ujf-grenoble.fr

Citation:
Rousset, B., R. Jolivet, M. Simons, C. Lasserre, B. Riel, P. Milillo, Z. Çakir, and F. Renard (2016), An aseismic slip transient on the North Anatolian Fault, *Geophys. Res. Lett.*, *43*, 3254–3262, doi:10.1002/2016GL068250.

Received 12 FEB 2016
Accepted 24 MAR 2016
Accepted article online 28 MAR 2016
Published online 14 APR 2016

An aseismic slip transient on the North Anatolian Fault

Baptiste Rousset[1], Romain Jolivet[2], Mark Simons[3], Cécile Lasserre[1], Bryan Riel[3], Pietro Milillo[3,4], Ziyadin Çakir[5], and François Renard[1,6]

[1]ISTerre, Université Grenoble Alpes, CNRS, IRD, Grenoble, France, [2]Laboratoire de Géologie, Département de Géosciences, École Normale Supérieure, PSL Research University, CNRS UMR, Paris, France, [3]Seismological Laboratory, Geological and Planetary Sciences, California Institute of Technology, Pasadena, California, USA, [4]School of Engineering, University of Basilicata, Potenza, Italy, [5]Department of Geology, Istanbul Technical University, Istanbul, Turkey, [6]Department of Geosciences, PGP, Blindern, University of Oslo, Oslo, Norway

Abstract Constellations of Synthetic Aperture Radar (SAR) satellites with short repeat time acquisitions allow exploration of active faults behavior with unprecedented temporal resolution. Along the North Anatolian Fault (NAF) in Turkey, an 80 km long section has been creeping at least since the 1944, M_w 7.3 earthquake near Ismetpasa, with a current Interferometric Synthetic Aperture Radar (InSAR)-derived average creep rate of 8 ± 3 mm/yr (i.e., a third of the NAF long-term slip rate). We use a dense set of SAR images acquired by the COSMO-SkyMed constellation to quantify the spatial distribution and temporal evolution of creep over 1 year. We identify a major burst of aseismic slip spanning 31 days with a maximum slip of 2 cm, between the surface and 4 km depth. This result shows that fault creep along this section of the NAF does not occur at a steady rate as previously thought, highlighting a need to revise our understanding of the underlying fault mechanics.

1. Introduction

Early observations of creep on strike slip faults were presented by *Steinbrugge et al.* [1960] for the central San Andreas Fault (SAF) and *Ambraseys* [1970] for the North Anatolian Fault (NAF). Using boreholes strain meter observations, *Linde et al.* [1996] made among the first inferences of finite duration slow slip transients made along the SAF. Since these results, studies of slow slip events have largely been focused on subduction zones [e.g., *Dragert et al.*, 2001; *Rogers and Dragert*, 2003; *Pritchard and Simons*, 2006; *Kostoglodov et al.*, 2010; *Hirose et al.*, 2010; *Ide et al.*, 2007; *Peng and Gomberg*, 2010]. Geodetic detection of slow aseismic transients along strike slip faults have been limited to the SAF [e.g., *Linde et al.*, 1996; *Murray and Segall*, 2005; *De Michele et al.*, 2011; *Khoshmanesh et al.*, 2015], the Superstition Hills Fault [*Wei et al.*, 2009], and the Haiyuan Fault [*Jolivet et al.*, 2013, 2015a]. Creepmeter measurements have highlighted very shallow transient events both on the SAF [*Schulz et al.*, 1982] and the NAF [*Altay and Sav*, 1991]. Indirect observations such as tremors or low-frequency earthquakes (LFEs) suggest that such behavior should be widespread [e.g., *Shelly*, 2015]. Geodetic studies using continuous Global Positioning System (cGPS) or (InSAR) greatly increase our ability to discriminate between creeping and locked portions of active continental faults [e.g., *Tong et al.*, 2013; *Cetin et al.*, 2014; *Thomas et al.*, 2014; *Jolivet et al.*, 2015b]. However, without a sufficiently dense cGPS network or short repeat time SAR observations, one can only derive average creep rates over the interseismic period.

We focus here on the study of the NAF, a major right-lateral fault accommodating the relative motion between the Anatolian and Eurasian Plates at a rate of 25 mm/yr [*McClusky et al.*, 2000]. More than 800 km of the fault ruptured during a westward propagating sequence of nine major earthquakes from 1939 to 1999 [e.g., *Ambraseys*, 1970; *Sengör*, 1979; *Stein et al.*, 1997] (Figure 1). At least two sections of the NAF are currently sliding aseismically: a 60 km long segment along the rupture of the 1999 Izmit earthquake [*Cakir et al.*, 2012] and an 80 km long segment along the rupture of the 1944 M_w 7.3, and 1951 M_w 6.9, earthquakes near Ismetpasa [*Cakir et al.*, 2005] (Figure 1). The Ismetpasa segment is currently seismically quiescent, and no tremors or LFEs have been detected from the existing local seismological networks [*Pfohl et al.*, 2015]. Using observations of bent railroad tracks in the 6 years following the 1944 earthquake, *Ambraseys* [1970] derived a 50 mm/yr creep rate along this segment in the early 1950s. Present-day creep rates of about 8 mm/yr are estimated using cGPS or InSAR data over 10 years [*Cakir et al.*, 2005; *Kaneko et al.*, 2013; *Cetin et al.*, 2014].

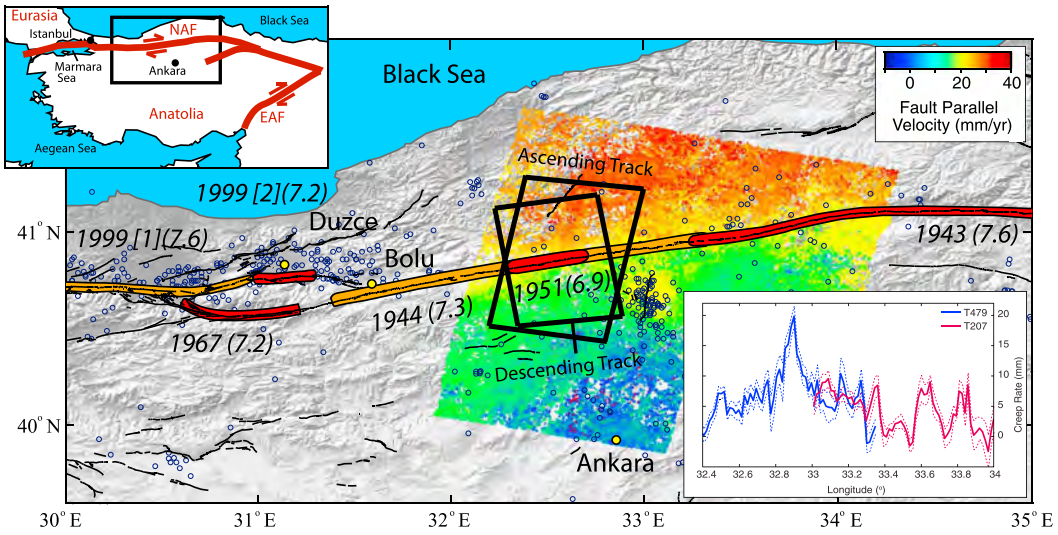

Figure 1. Tectonic setting of the study area. Red and orange ellipses correspond to major earthquakes that ruptured the western NAF during the last century: the 1943 M_w 7.6 Tosia-Ladik earthquake, the 1944 M_w 7.3 Bolu-Gerede earthquake, the 1951 M_w 6.9 Kurşunlu earthquake, the 1967 M_w 7.2 Mudurnu earthquake, and the 1999 M_w 7.6 Izmit and M_w 7.2 Düzce earthquakes. Dark blue dots correspond to the microseismicity from 1990 to 2015 recorded in the Kandilli earthquake catalog ($M > 2.5$). The color image corresponds to the permanent scatter-derived average velocities from Envisat acquisitions between 2003 and 2011 [*Cetin et al.*, 2014]. Black rectangles indicate the ascending and descending CSK tracks considered in this study. Bottom right: Creep rate along the fault for the two Envisat tracks [*Cetin et al.*, 2014]. Top left: Large-scale geodynamic context indicating the two main strike-slip faults that delineate the Anatolian block: the East Anatolian Fault (EAF) and the NAF.

Thus, estimates made in the intervening 50 years suggest the creep rate decreased dramatically following the 1944 rupture, revealing a long-lived postseismic afterslip sequence [*Cetin et al.*, 2014]. The spatial coincidence of large M_w 7 seismic ruptures, rapid afterslip over a 50 year period and steady creep over the last 15 years may be explained by a bimodal depth distribution of frictional properties on the fault. Velocity strengthening properties are required at shallow depths, which is consistent with the lithology observed in the fault gouge [*Kaduri et al.*, 2015], as well as velocity weakening properties at depths larger than 3 to 6 km [*Kaneko et al.*, 2013].

We report on a transient episode of aseismic slip on the Ismetpasa segment that has been detected using a dense set of radar images acquired by the COSMO-SkyMed (CSK) constellation of satellites. We consider interferograms on two orbital tracks, one ascending and one descending, using time series analysis to derive the temporal evolution of creep along a 20 km long segment in the vicinity of Ismetpasa. We use a Bayesian approach to derive the extent and amplitude of slip at depth and discuss possible mechanical implications of such a transient episode.

2. InSAR Data and Time Series Analysis Reveal a Transient Episode of Creep

We processed two sets of interferograms using X band acquisitions from the CSK four satellites constellation spanning from July 2013 to May 2014. On the ascending track, we formed 140 interferograms involving 49 separate acquisitions (Figure S1 in the supporting information), and on the descending track, we formed 65 interferograms using 20 separate acquisitions (Figure S2). We computed interferograms using the InSAR Scientific Computing Environment (ISCE) software (Jet Propulsion Laboratory (JPL)/Caltech, [*Rosen et al.*, 2012]). Based on an empirical evaluation of interferometric coherence, we consider pairs with perpendicular baselines smaller than 400 m and temporal baselines shorter than 40 days. We correct for the topographic component of the interferometric phase using the Advanced Spaceborne Thermal Emission and Reflection Radiometer (ASTER) 30 m pixel spacing digital elevation model [*Abrams*, 2000]. We unwrap interferograms using the ICU software [*Goldstein et al.*, 1988]. Within individual interferograms, coherence is high. However, patterns corresponding to strong atmospheric phase delays are common and obvious. In some places, these phase delays, on the order of one to several centimeters, correlate with topography (Figure 2), and are related

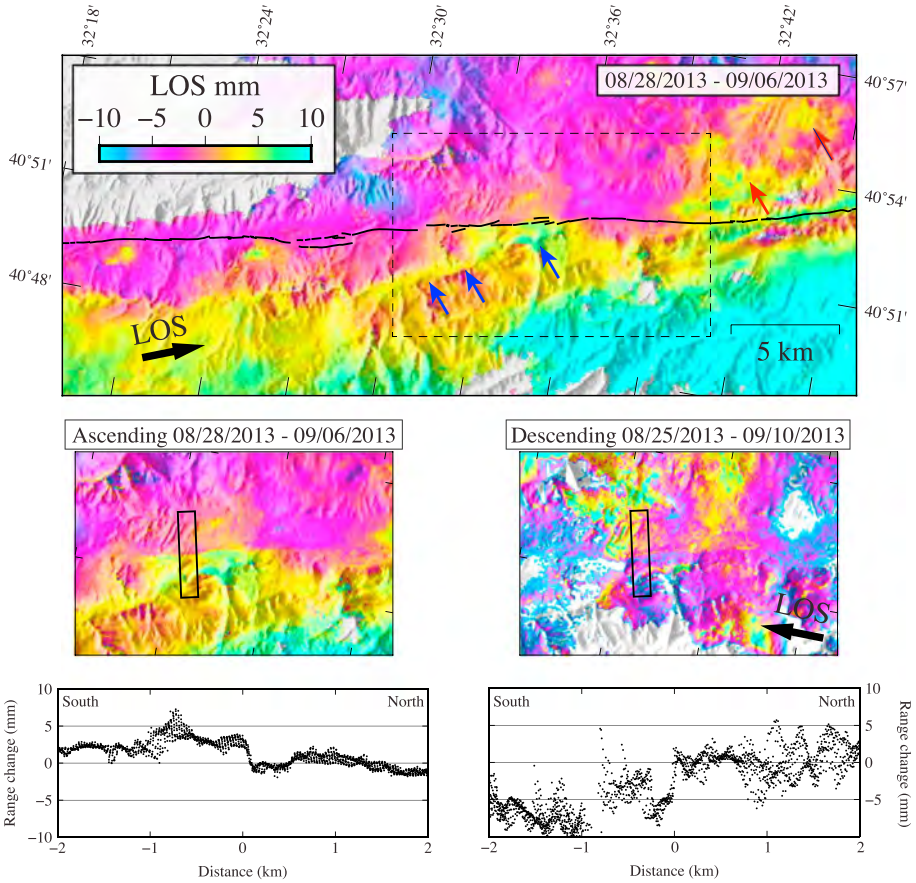

Figure 2. Example interferograms that capture a strong phase gradient on the fault trace. (top) Interferogram of the ascending track spanning 28 August 2013 to 6 September 2013. Note the presence of path delay effects presumed to be due to turbulence in the atmosphere. (middle left) Zoom of the top interferogram on the fault without the fault trace. (middle right) Same left zoom, but for the descending interferogram spanning 25 August 2013 to 10 September 2013. (bottom row) 4 km long and 1 km wide profiles perpendicular to the fault for the ascending and descending interferograms.

to spatiotemporal variations in the stratification of the troposphere. In other examples, we find significant spatially correlated phase variations that we associate with turbulent troposphere (Figure 2).

Many of the interferograms image a clear discontinuity in the interferometric phase occurring along the North Anatolian Fault (Figure 2). This discontinuity is visible on multiple interferograms using independent acquisitions and is therefore not a propagation artifact. The high strain gradient centered on the fault suggests shallow fault slip. The discontinuity extends for 5 to 8 km along the fault trace and is visible on both ascending and descending track data. As the sign of the phase gradient is opposite on ascending and descending interferograms, we conclude that slip along the fault is primarily horizontal. Also, as we do not see this discontinuity either before or after the August–September 2013 period, thus, this deformation signal is presumed to be the signature of a transient episode of right-lateral slip reaching the surface of the NAF.

In order to characterize the amplitude, timing, and spatial extent of this transient slip at depth and along strike, we consider a time series analysis of surface deformation. The combination of a time series approach and the short repeat times provided by the CSK constellation (i.e., variable from 1 to 16 days) allows us to reduce noise and detect small-amplitude deformation signals. We first calculate and remove phase delays corresponding to the temporal variability in the stratified atmosphere by estimating on each individual unwrapped interferogram an empirical relationship between phase and topography, determined using multiple spatial wavelengths [*Lin et al.*, 2010]. We also estimate empirically residual orbital errors by fitting a plane to each interferogram. Orbital errors and atmospheric corrections are adjusted to be consistent within the interferometric network [*Lin et al.*, 2010]. We then use the New Small Baseline (NSBAS) scheme implemented in the

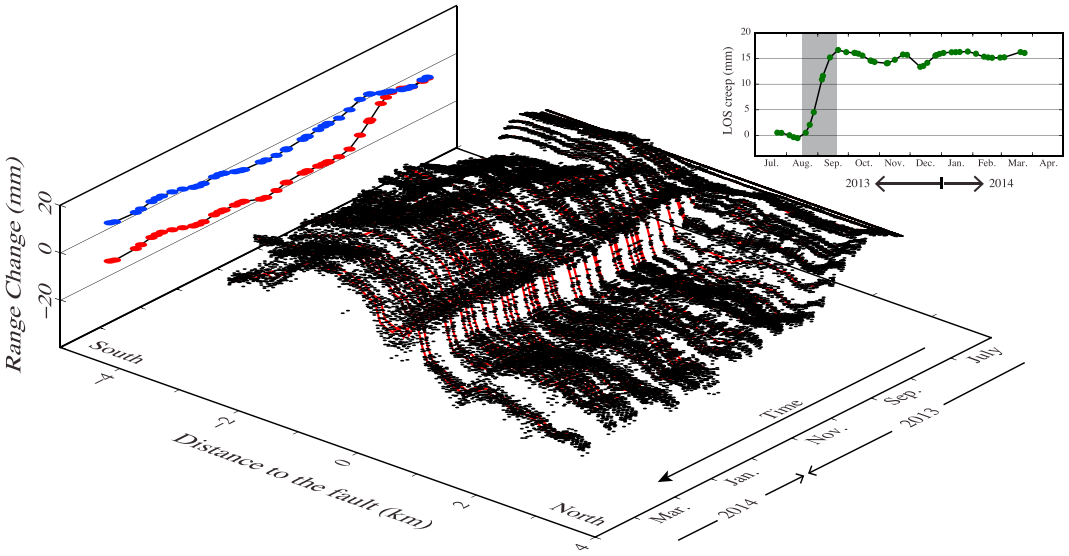

Figure 3. Fault perpendicular profiles of LOS surface displacement versus time. The main plot shows the temporal evolution between July 2013 and April 2014 of surface range displacement on a 500 m wide and 8 km long profile centered on the fault. Blue (south) and red (north) dots curves show average range change taken from two 100 m wide swaths located 300 m apart from each others on each side of the fault. Top right: Difference between the blue and the red curves. The period of transient creep is highlighted by the grey rectangle spanning from August to September 2013.

Generic Interferometric Analysis Toolbox (GIAnT) [*Doin et al.*, 2011; *Jolivet et al.*, 2012; *Agram et al.*, 2013]. We estimate the line-of-sight (LOS) phase evolution for each pixel independently, by solving the set of equations that links the phase difference of an interferogram to the corresponding acquisition dates and by adding a constant velocity constraint to link unconnected networks of interferograms. We eventually remove all the pixels for which the difference between the raw data and the reconstructed value is higher than 2 mm. In the following, we concentrate on observations from the ascending track. Although data from the descending track do not contradict our findings, the smaller number of independent acquisitions compared to ascending data, as well as their higher level of noise, make the resulting time series less robust than that from the ascending data (supporting information Figure S3).

Figure 3 shows the temporal evolution of a fault perpendicular profile of the LOS displacement derived from the time series analysis. A clear transient creep event is visible between the acquisition dates of 20 August and 21 September 2013, during which six images were acquired. In the month before this period and the six months after, we cannot detect any obvious signal across the fault. This observation suggests that near the surface, the fault only creeps during 1 month out of the 10 spanned by the CSK data. The cumulative offset across the fault extracted from this fault perpendicular profile reaches 1.5 cm in the LOS direction. Assuming slip is purely horizontal, this offset corresponds to about 2 cm of right-lateral fault slip (with an incidence angle of 49°, a fault strike of 70°, and a heading of 13°W). This amount of transient slip is equivalent to 2.5 years of steady creep at the average rate of ~8 mm/yr measured by InSAR over 10 years using Envisat data [*Cetin et al.*, 2014] or to 1 year of the total differential motion between the Eurasian and Anatolian Plates. This observation is the first evidence from InSAR that creep on the Ismetpasa segment is not steady but may occur through a succession of transient episodes of slip of significant size. The 5–8 km along-strike extent and the amount of slip involved (2 cm) suggests that the observed creep event affects more than just the shallowest (i.e., first 100 m) portion of the NAF and presumably extends to significant depths. To explore this question further, we develop a model of distributed subsurface fault creep.

3. Slip Distribution of the Creep Burst

Imaging slip on the fault interface consists in inverting the forward problem, $\mathbf{d} = \mathbf{Gm}$, where $\mathbf{d}$ is the vector of the LOS surface displacements at all pixels between acquisition dates 20 August 2013 and 21 September 2013 reconstructed from the time series analysis, $\mathbf{m}$ is the vector of slip on the discretized fault plane,

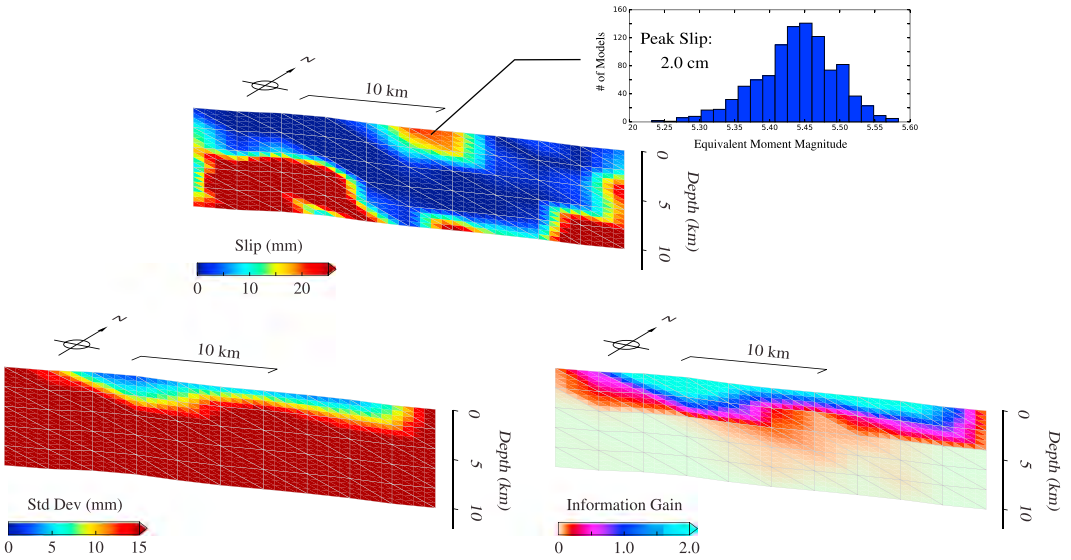

Figure 4. Slip models for the 2013 creep burst along the North Anatolian Fault. (top) Mode of the posterior probability density function (PDF) of total slip during the 2013 creep event. Note that deeper high slip patterns are not constrained and only reflect the mode of the prior. The top right inset presents the posterior PDF of the slipping area corresponding to the creep burst with the number of models that explain the data as a function of the equivalent moment magnitude. (bottom left) Standard deviation of the PDF of slip during the 2013 creep event. (bottom right) Kullback-Leibler divergence of the PDF of slip computed using the prior likelihood (i.e., uniform distributions between 0 and 6 cm) and the posterior PDF. Higher values indicate regions where the gain of information of the posterior PDF is significant relative to the prior distribution.

and **G** is the matrix of the Green's functions (i.e., the surface elastic response to unit displacement on each point of the fault). We downsample the LOS map of surface displacements to 920 data points using a quad-tree downsampling approach maximizing the resulting resolution on our fault plane (see Figure S6 and *Lohman and Simons* [2005]). We compute the Green's functions for a semi-infinite stratified elastic medium using the EDKS software [*Simons et al.*, 2002]. The elastic moduli are derived from the V_p model used by H. Karabulut (personal communication) to locate microseismicity in this area (see supporting information Table S1). The fault model geometry is assumed vertical and follows the mapped trace of the NAF, with nodes equally spaced every 2 km. **m** corresponds to slip at each node of the triangular fault mesh. Slip on the fault is the linear interpolation of the amplitude of slip at each node. Given that we only consider one LOS data set and that slip is mostly horizontal, we only solve for the along-strike component of slip. In addition, as the displacement map we recover from the time series analysis shows residual atmospheric patterns correlated with topography, we simultaneously solve for a linear relationship between displacement and topography. Finally, we include a linear function of azimuth and range to account for possible orbital residuals.

Our noise model includes the contribution of turbulent atmospheric noise by incorporating an empirically estimated covariance function of the displacement data used to build the data covariance matrix $\mathbf{C}_d$. This function parameterizes the correlation between data points to be an exponential function of the separation distance, decreasing as a function of distance between observables, with a characteristic length scale of 2 km and an amplitude of 3 mm (Figure S4). In addition to $\mathbf{C}_d$, we account for 5% uncertainty in the elastic parameters of our stratified elastic medium by constructing the prediction error covariance matrix, $\mathbf{C}_p$, following the approach of *Duputel et al.* [2014]. A standard way to obtain a slip model is to use a constrained least squares inversion (as presented for comparison purposes in supporting information Figure S5 and corresponding text). However, this inversion method requires arbitrary choices for regularization. To provide an ensemble of plausible models, we instead adopt an unregularized Bayesian approach and derive the probability density function (PDF) of slip on the fault, $p(\mathbf{m}|\mathbf{d})$. This posterior PDF is proportional to the prior PDF of slip (i.e., the state of knowledge we have on the slip before we bring in any information from data), $p(\mathbf{m})$, and to the data likelihood, $p(\mathbf{d}|\mathbf{m})$, such that

$$p(\mathbf{m}|\mathbf{d}) \propto p(\mathbf{m}) \exp\left[-\frac{1}{2}(\mathbf{d}-\mathbf{Gm})^T \mathbf{C}_\chi^{-1}(\mathbf{d}-\mathbf{Gm})\right] \quad (1)$$

where $\mathbf{C}_\chi$ is the misfit covariance matrix, which we approximate as the sum of $\mathbf{C}_d$ and $\mathbf{C}_p$ [*Duputel et al.*, 2014]. We infer the posterior PDF $p(\mathbf{m}|\mathbf{d})$ using AlTar, a reimplementation of the Cascading Adaptive Transitional Metropolis In Parallel (CATMIP) [*Minson et al.*, 2013] sampling algorithm.

We consider the mode of posterior PDF of slip on the fault, together with the standard deviation of slip and the information gain criterion (Figure 4). To quantify the information gain, we estimate the Kullback-Leibler Divergence (D^i_{KL}), a criterion relative to the prior PDF defined as $D^i_{\mathrm{KL}} = \int_{\mathbf{m}} p(m^i|\mathbf{d}) \ln(\frac{p(m^i|\mathbf{d})}{p(m^i)})$, where $p(m^i)$ and $p(m^i|\mathbf{d})$ are the marginals of the prior and posterior PDF for parameter m^i. D^i_{KL} is always positive or equal to zero. $D^i_{\mathrm{KL}} = 0$ corresponds to the posterior PDF being equal to the prior PDF, i.e., $p(m^i|\mathbf{d}) = p(m^i)$, implying that we are not able to extract information for this part of the model given our data. In Figure 4 (top), the patch of slip corresponding to the observed surface displacement is localized between the surface and 2 to 4 km depth where standard deviations are lower than 1.0 cm, with a peak slip of 2.0 cm at the surface. The slip pattern is asymmetrical and presents more slip at depth on its eastern end. The posterior PDF of slip in the lower part of the fault is similar to the prior PDF, showing that we have insufficient information to constrain slip at such depths. The significant gain of information is broadly limited to the upper 4 km of the fault, except in a limited region in the middle of the model where some information is extracted down to 6 to 8 km.

Marginal PDFs of slip along strike at various depths confirm that we can locate the slip event in the first 4 km. At greater depths, posterior PDFs are uniform and similar to the prior PDFs assumed (see supporting information Figures S8 and S9). Our inversion formulation also enables to quantify probabilities for the main parameters of the slip pattern. For example, considering the nodes with $D^i_{KL} > 1.0$ and immediate neighbors, we can infer an 82% probability that 70% of the slip potency is concentrated at depths shallower than 3 km. For the same set of nodes, we derive a 72% probability that the peak slip is localized between 1 and 4 km depth. Finally, we derive the PDF of the total equivalent moment of the aseismic event, which we find to lie between 1e17 to 3e17 N m, corresponding to an equivalent moment magnitude of 5.2 to 5.5 (Figure 4).

4. Discussion

During the 10 months period of observation and for the 50 km long fault section studied here, the CSK data and the derived slip model indicate that creep is episodic rather than steady. We have processed additional adjacent tracks eastward, along more than 120 km of the fault, and we do not observe other creep bursts. This other data set has a higher noise level, which may prevent from any detection of temporal fluctuations of creep. However, these observations do not show evidence of creep at all, although we would expect approximately 6 mm of creep to have built up along the fault over our period of observations. The question then arises whether creep was episodic in the past as well. During the early postseismic period, when the creep rate on the Ismetpasa segment was as high as 50 mm/yr, a 1 month transient event accounting for 2 years of average creep would have had a peak slip of 10 cm. However, no continuous observations were available at that time to detect such type of events. Creepmeter measurements made in the 1980s suggest that 1 month transients were already present [*Altay and Sav*, 1991]. However, these observations can be sensitive to shallow processes (e.g., rainfall), and thus the extent to which those observations are of significant tectonic origin remains ambiguous. Furthermore, it is not possible to estimate the depth extent of these fault movements with only creepmeter measurements. During the Envisat and (ALOS) InSAR observation period, it may also have been difficult to detect short lived transients given the limited temporal sampling. Indeed, on average, only four ALOS acquisitions are available per year over the 2007–2011 period [*Kaneko et al.*, 2013] and three Envisat acquisitions per year over the 2003–2011 period [*Cetin et al.*, 2014]. Also, the average creep rate appears to be decreasing since the 1944 earthquake [e.g., *Cetin et al.*, 2014]. If we hypothesize that the tendency to have transient slip behavior increases as loading rate decreases, then it is possible that no transients slip event have occurred before the one described herein. Alternatively, such transients have occurred but went unobserved.

Average velocity maps and creep models constrained from InSAR data between 2003 and 2011 along the Ismetpasa creeping section suggest that creep along the NAF is restricted within the uppermost 5 to 7 km depth. The creep event that we detected is located at similar depths. If representative of the fault behavior, such type of creep events could contribute to build the average creep signal previously observed with a sparser set of images. The event described here corresponds to about 2 cm of slip at its peak, or more than 2 years of average creep as observed by other InSAR studies [*Kaneko et al.*, 2013; *Cetin et al.*, 2014].

If similar events were to occur along this segment, the recurrence between events would be ~2 years, perhaps explaining why we do not detect any other event in the 10 months of data currently available to us.

Whether or not slip was occurring as transients in the past decades, the episode of slip described in this study raises the question of the validity of existing simple mechanical models. In the laterally homogeneous model proposed by *Kaneko et al.* [2013], earthquakes nucleating in a 5 to 15 km depth slip weakening region propagate through the slip strengthening region at the surface. As the peak coseismic slip for the modeled 1944 earthquake is not at the surface, the top 5 km experience a sudden shear stress increase which is released by several decades of decaying postseismic slip. The *Kaneko et al.* [2013] model also predicts that presently, either the yearly average creep rate is decreasing very slowly or slip is perpetuated by steady creep. However, our observations suggest creep is not just long lived but could be a succession of monthly creep transients separated by locking periods. Therefore, we need a model that allows for full locking at the surface and spontaneous generation of episodes of creep, as also reproduced in laboratory experiments of slow propagation of a crack front [*Schmittbuhl and Måløy*, 1997]. Such events are observed in the vicinity of seismic (i.e., rate weakening) asperities, where the largest stress gradients are observed, in numerical models of the earthquake cycle using a frictional description of faults [*Lapusta and Liu*, 2009; *Barbot et al.*, 2012]. A more complex tuning of this empirical formalism than done by *Kaneko et al.* [2013] may potentially reproduce this behavior, such as the one made by *Wei et al.* [2013] for the SAF with a conditionally stable layer at depths of shallow transient events. While tuning the rate-and-state formalism might explain the transient nature of slip in this case, the underlying physical mechanisms still remain unknown.

Another feature of an improved model should account for the elastic loading of the shallow portion of the fault. If we consider that postseismic slip has now released most of the stress perturbation induced by the earthquake (on the order of 1 MPa), stress needs to build up at shallow depth until the generation of a transient episode of slip. Shear stressing rate imposed on the fault at the surface by a vertical dislocation in an elastic half-space, at a depth d with a slip rate $\dot{s}$, is expressed as $\tau = \frac{\mu \dot{s}}{2\pi d}$, with μ the elastic shear modulus [*Savage and Burford*, 1973]. Assuming that the seismogenic portion of the fault is fully locked at depth shallower than d, ranging from 10 to 20 km, with slip rates between 2 and 3 cm/yr and $\mu = 30$ GPa, the shear stressing rate at the surface is between 5 and 15 kPa/yr. In the same model, shear stress associated with the transient is expressed as $\tau_t = \frac{\mu s_t}{2\pi d_t}$, where s_t is the slip and d_t is the maximum depth of the transient. Assuming a depth, d_t, of 4 km and a slip, s_t, of 2 cm, the stress drop of the transient is 24 kPa. Therefore, with a locking depth between 10 and 20 km, it would take between 2 and 5 years to account for a transient similar to that observed. Note that this simple calculation does not account for three-dimensional effects but provides an order of magnitude for this type of event.

The aseismic slip transient event described here was generated spontaneously and did not accelerate to generate an earthquake. We have not identified any external process that could have triggered this event. Since loading and unloading cycles of aquifers have been suggested to play a role in the seismic and aseismic behavior of faults [e.g., *González et al.*, 2012], we considered precipitation data from the Tropical Rainfall Measuring Mission (TRMM) satellite. However, there is no significant rainfall before the creep event (Figure S10). In addition, no significant seismic event in the vicinity of this segment has been recorded and no large earthquake in the region or large teleseismic earthquake occurred during this period of time. The triggering of slip events along active faults by local or remote earthquakes has been observed [*Zigone et al.*, 2012; *Tape et al.*, 2013; *Wei et al.*, 2015] but cannot explain the origin of this creep burst (see Figure S11 for an analysis of the local seismicity).

5. Conclusion

We detected a month-long transient aseismic creep event along the Ismetpasa section of the North Anatolian Fault using a temporally dense InSAR time series analysis. We infer a distribution of slip corresponding to this event using a Bayesian approach that accounts for errors in both data and assumed forward model. The peak slip of this burst is ~ 2 cm, equivalent to 1 year of tectonic loading. Prior to this study, the Ismetpasa creeping section was thought to slip at a constant rate of 8 mm/yr, after a period of exponential decay of the creep rate following the 1944 earthquake. As we have not found a cause for a sudden shear stress increase or normal stress decrease right before this transient slip event, the observed velocity increase is not consistent with simple velocity strengthening fault constitutive parameters. We consider two scenarios for reconciling these observations: (1) creep has never been steady and prior observations that could not untangle the rich

temporal behavior of creep, made of slow slip events interacting with each other [*Jolivet et al.*, 2015a], and (2) creep was steady and has now become episodic. In both cases, refining the fault zone properties and mechanical model is needed to explain such transient episodes of slip and to understand the regional seismogenic behavior of the NAF.

Acknowledgments
We used the original COSMO-SkyMed product (copyright ASI -Agenzia Spaziale Italiana, 2013–2016) and processed the acquisitions using the ARIA and ISCE systems developed at JPL/Caltech. COSMO-SkyMed data products are processed at JPL under license from ASI as part of a collaborative project between CIDOT and JPL/Caltech. We thank the French Labex OSUG@2020 for support of B.R. during a visit to Caltech. M.S. was supported by NSF grant EAR-1447107. We also acknowledge support from the ALEAS program (INSU-CNRS). We are grateful to Michel Bouchon and Hyrullah Karabulut for stimulating discussions. We thank the Editor A. Newman and two anonymous reviewers for the constructive comments.

References

Abrams, M. (2000), The Advanced Spaceborne Thermal Emission and Reflection Radiometer (ASTER): Data products for the high spatial resolution imager on NASA's Terra platform, *Int. J. Remote Sens.*, *21*(5), 847–859.

Agram, P., R. Jolivet, B. Riel, Y. Lin, M. Simons, E. Hetland, M.-P. Doin, and C. Lasserre (2013), New radar interferometric time series analysis toolbox released, *Eos Trans. AGU*, *94*(7), 69–70.

Altay, C., and H. Sav (1991), Continuous creep measurement along the North Anatolian Fault zone, *Bull. Geol. Congr. Turkey*, *6*, 77–84.

Ambraseys, N. (1970), Some characteristic features of the Anatolian Fault Zone, *Tectonophysics*, *9*(2), 143–165.

Barbot, S., N. Lapusta, and J. P. Avouac (2012), Under the hood of the earthquake machine: Toward predictive modeling of the seismic cycle, *Science*, *336*(6082), 707–710.

Cakir, Z., A. M. Akoglu, S. Belabbes, S. Ergintav, and M. Meghraoui (2005), Creeping along the Ismetpasa section of the North Anatolian Fault (Western Turkey): Rate and extent from InSAR, *Earth Planet. Sci. Lett.*, *238*(1), 225–234.

Cakir, Z., S. Ergintav, H. Özener, U. Dogan, A. M. Akoglu, M. Meghraoui, and R. Reilinger (2012), Onset of aseismic creep on major strike-slip faults, *Geology*, *40*(12), 1115–1118.

Cetin, E., Z. Cakir, M. Meghraoui, S. Ergintav, and A. M. Akoglu (2014), Extent and distribution of aseismic slip on the Ismetpaşa segment of the North Anatolian Fault (Turkey) from persistent scatterer InSAR, *Geochem. Geophys. Geosyst.*, *15*(7), 2883–2894.

De Michele, M., D. Raucoules, F. Rolandone, P. Briole, J. Salichon, A. Lemoine, and H. Aochi (2011), Spatiotemporal evolution of surface creep in the Parkfield region of the San Andreas Fault (1993–2004) from synthetic aperture radar, *Earth Planet. Sci. Lett.*, *308*(1), 141–150.

Doin, M.-P., S. Guillaso, R. Jolivet, C. Lasserre, F. Lodge, G. Ducret, and R. Grandin (2011), Presentation of the small baseline NSBAS processing chain on a case example: The Etna deformation monitoring from 2003 to 2010 using Envisat data, paper presented at European Space Agency "Fringe" Symposium, Frascati, Italy, 19–23 Sept.

Dragert, H., K. Wang, and T. S. James (2001), A silent slip event on the deeper Cascadia subduction interface, *Science*, *292*(5521), 1525–1528.

Duputel, Z., P. S. Agram, M. Simons, S. E. Minson, and J. L. Beck (2014), Accounting for prediction uncertainty when inferring subsurface fault slip, *Geophys. J. Int.*, *197*, 464–482.

Goldstein, R. M., H. A. Zebker, and C. L. Werner (1988), Satellite radar interferometry: Two-dimensional phase unwrapping, *Radio Sci.*, *23*(4), 713–720.

González, P. J., K. F. Tiampo, M. Palano, F. Cannavó, and J. Fernández (2012), The 2011 Lorca earthquake slip distribution controlled by groundwater crustal unloading, *Nat. Geosci.*, *5*(11), 821–825.

Hirose, H., Y. Asano, K. Obara, T. Kimura, T. Matsuzawa, S. Tanaka, and T. Maeda (2010), Slow earthquakes linked along dip in the Nankai subduction zone, *Science*, *330*(6010), 1502–1502.

Ide, S., G. C. Beroza, D. R. Shelly, and T. Uchide (2007), A scaling law for slow earthquakes, *Nature*, *447*(7140), 76–79.

Jolivet, R., C. Lasserre, M.-P. Doin, S. Guillaso, G. Peltzer, R. Dailu, J. Sun, Z.-K. Shen, and X. Xu (2012), Shallow creep on the Haiyuan fault (Gansu, China) revealed by SAR interferometry, *J. Geophys. Res.*, *117*, B06401, doi:10.1029/2011JB008732.

Jolivet, R., C. Lasserre, M. P. Doin, G. Peltzer, J. P. Avouac, J. Sun, and R. Dailu (2013), Spatio-temporal evolution of aseismic slip along the Haiyuan fault, China: Implications for fault frictional properties, *Earth Planet. Sci. Lett.*, *377–378*, 23–33.

Jolivet, R., T. Candela, C. Lasserre, F. Renard, Y. Klinger, and M. P. Doin (2015a), The burst-like behavior of aseismic slip on a rough fault: The creeping section of the Haiyuan Fault, China, *Bull. Seismol. Soc. Am.*, *105*(1), 480–488.

Jolivet, R., M. Simons, P. Agram, Z. Duputel, and Z.-K. Shen (2015b), Aseismic slip and seismogenic coupling along the central San Andreas Fault, *Geophys. Res. Lett.*, *42*, 297–306, doi:10.1002/2014GL062222.

Kaduri, M., F. Renard, J.-P. Gratier, Z. Çakir, and C. Lasserre (2015), The implication of gouge mineralogy evolution on fault creep: An example from the North Anatolian Fault, Turkey, Abstracts MR33C-2678 presented at 2015 Fall Meeting, AGU, San Francisco, Calif., 14–48 Dec.

Kaneko, Y., Y. Fialko, D. Sandwell, X. Tong, and M. Furuya (2013), Interseismic deformation and creep along the central section of the North Anatolian Fault (Turkey): InSAR observations and implications for rate-and-state friction properties, *J. Geophys. Res. Solid Earth*, *118*, 316–331, doi:10.1029/2012JB009661.

Khoshmanesh, M., M. Shirzaei, and R. Nadeau (2015), Time-dependent model of aseismic slip on the central San Andreas Fault from InSAR time series and repeating earthquakes, *J. Geophys. Res. Solid Earth*, *120*, 6658–6679, doi:10.1002/2015JB012039.

Kostoglodov, V., A. Husker, N. M. Shapiro, J. S. Payero, M. Campillo, N. Cotte, and R. Clayton (2010), The 2006 slow slip event and nonvolcanic tremor in the Mexican subduction zone, *Geophys. Res. Lett.*, *37*, L24301, doi:10.1029/2010GL045424.

Lapusta, N., and Y. Liu (2009), Three-dimensional boundary integral modeling of spontaneous earthquake sequences and aseismic slip, *J. Geophys. Res.*, *114*, B09303, doi:10.1029/2008JB005934.

Lin, Y.-N. N., M. Simons, E. A. Hetland, P. Muse, and C. DiCaprio (2010), A multiscale approach to estimating topographically correlated propagation delays in radar interferograms, *Geochem. Geophys. Geosyst.*, *11*, Q09002, doi:10.1029/2010GC003228.

Linde, A. T., M. T. Gladwint, M. J. Johnston, R. L. Gwythert, and R. G. Bilham (1996), A slow earthquake sequence on the San Andreas Fault, *Nature*, *383*, 65–68.

Lohman, R. B., and M. Simons (2005), Some thoughts on the use of InSAR data to constrain models of surface deformation: Noise structure and data downsampling, *Geochem. Geophys. Geosyst.*, *6*, Q01006, doi:10.1029/2004GC000841.

McClusky, S., et al. (2000), Global Positioning System constraints on plate kinematics and dynamics in the eastern Mediterranean and Caucasus, *J. Geophys. Res.*, *105*(B3), 5695–5719.

Minson, S., M. Simons, and J. Beck (2013), Bayesian inversion for finite fault earthquake source models. I—Theory and algorithm, *Geophys. J. Int.*, *194*, 1701–1726.

Murray, J. R., and P. Segall (2005), Spatiotemporal evolution of a transient slip event on the San Andreas fault near Parkfield, California, *J. Geophys. Res.*, *110*, B09407, doi:10.1029/2005JB003651.

Peng, Z., and J. Gomberg (2010), An integrated perspective of the continuum between earthquakes and slow-slip phenomena, *Nat. Geosci.*, *3*(9), 599–607.

Pfohl, A., L. M. Warren, S. Sit, and M. Brudzinski (2015), Search for tectonic tremor on the central North Anatolian Fault, Turkey, *Bull. Seismol. Soc. Am.*, *105*(3), 1779–1786.

Pritchard, M., and M. Simons (2006), An aseismic slip pulse in northern Chile and along-strike variations in seismogenic behavior, *J. Geophys. Res.*, *111*, B8405, doi:10.1029/2006JB004258.

Rogers, G., and H. Dragert (2003), Episodic tremor and slip on the Cascadia subduction zone: The chatter of silent slip, *Science*, *300*(5627), 1942–1943.

Rosen, P. A., E. Gurrola, G. F. Sacco, and H. Zebker (2012), The InSAR scientific computing environment, paper presented at 9th European Conference on Synthetic Aperture Radar, EUSAR 2012, VDE, pp. 730–733, Nürnberg, Germany, 23–26 Apr.

Savage, J. C., and R. O. Burford (1973), Geodetic determination of relative plate motion in central California, *J. Geophys. Res.*, *78*(5), 832–845.

Schmittbuhl, J., and K. J. Måløy (1997), Direct observation of a self-affine crack propagation, *Phys. Rev. Lett.*, *78*(20), 3888–3891.

Schulz, S. S., G. M. Mavko, R. O. Burford, and W. D. Stuart (1982), Long-term fault creep observations in central California, *J. Geophys. Res.*, *87*(B8), 6977–6982.

Sengör, A. (1979), The North Anatolian transform fault: Its age, offset and tectonic significance, *J. Geol. Soc.*, *136*(3), 269–282.

Shelly, D. R. (2015), Complexity of the deep San Andreas Fault zone defined by cascading tremor, *Nat. Geosci.*, *8*(2), 145–151.

Simons, M., Y. Fialko, and L. Rivera (2002), Coseismic deformation from the 1999 M_w 7.1 Hector Mine, California, earthquake as inferred from InSAR and GPS observations, *Bull. Seismol. Soc. Am.*, *92*(4), 1390–1402.

Stein, R. S., A. A. Barka, and J. H. Dieterich (1997), Progressive failure on the North Anatolian Fault since 1939 by earthquake stress triggering, *Geophys. J. Int.*, *128*(3), 594–604.

Steinbrugge, K. V., E. G. Zacher, D. Tocher, C. Whitten, and C. Claire (1960), Creep on the San Andreas Fault, *Bull. Seismol. Soc. Am.*, *50*(3), 389–415.

Tape, C., M. West, V. Silwal, and N. Ruppert (2013), Earthquake nucleation and triggering on an optimally oriented fault, *Earth Planet. Sci. Lett.*, *363*, 231–241.

Thomas, M. Y., J.-P. Avouac, J. Champenois, J.-C. Lee, and L.-C. Kuo (2014), Spatiotemporal evolution of seismic and aseismic slip on the Longitudinal Valley Fault, Taiwan, *J. Geophys. Res. Solid Earth*, *119*, 5114–5139, doi:10.1002/2013JB010603.

Tong, X., D. Sandwell, and B. Smith-Konter (2013), High-resolution interseismic velocity data along the San Andreas Fault from GPS and InSAR, *J. Geophys. Res. Solid Earth*, *118*, 369–389, doi:10.1029/2012JB009442.

Wei, M., Y. Kaneko, Y. Liu, and J. J. McGuire (2013), Episodic fault creep events in California controlled by shallow frictional heterogeneity, *Nat. Geosci.*, *6*(7), 566–570.

Wei, M., Y. Liu, Y. Kaneko, J. J. McGuire, and R. Bilham (2015), Dynamic triggering of creep events in the Salton Trough, Southern California by regional $M \geq 5.4$ earthquakes constrained by geodetic observations and numerical simulations, *Earth Planet. Sci. Lett.*, *427*, 1–10.

Wei, M., D. Sandwell, and Y. Fialko (2009), A silent M_w 4.7 slip event of October 2006 on the Superstition Hills fault, southern California, *J. Geophys. Res.*, *114*, B07402, doi:10.1029/2008JB006135.

Zigone, D., et al. (2012), Triggering of tremors and slow slip event in Guerrero, Mexico, by the 2010 M_w 8.8 Maule, Chile, earthquake, *J. Geophys. Res.*, *117*, B09304, doi:10.1029/2012JB009160.